Annales Geophysicae (2002) 2002: 365–376 © European Geophysical Society 2002

Annales Geophysicae

Electrostatic interaction between Interball-2 and the ambient plasma. 1. Determination of the spacecraft potential from current calculations

M. Bouhram[1], **N. Dubouloz**[1, 2], **M. Hamelin**[1], **S. A. Grigoriev**[3], **M. Malingre**[1], **K. Torkar**[4], **M. V. Veselov**[5], **Y. Galperin**[5], **J. Hanasz**[6], **S. Perraut**[7], **R. Schreiber**[8], **and L. V. Zinin**[3]

[1]CETP-CNRS, 4 Avenue de Neptune, 94100 Saint-Maur, France
[2]LPCE-CNRS, 45071 Orleans Cedex, France
[3]Mathematical Dept., Kaliningrad State University, 236041 Kaliningrad, Russia
[4]Space Research Institute, A. A. S., Inffeldgasse 12, A-8010 Graz, Austria
[5]Space Research Institute, R. A. S., Profsoyuznaya 84/32, 117810 Moscow, Russia
[6]Space Research Centre, P. A. S., ul. Rabianska 8, 87-100 Torun, Poland
[7]CETP-CNRS, 10-12 Avenue de l'Europe, 78140 Velizy, France
[8]N. Copernicus Astronomical Centre, P. A. S., ul. Rabianska 8, 87-100 Torun, Poland

Received: 2 March 2001 – Revised: 20 November 2001 – Accepted: 12 December 2001

Abstract. The Interball-2 spacecraft travels at altitudes extending up to 20 000 km, and becomes positively charged due to the low-plasma densities encountered and the photoemission on its sunlit surface. Therefore, a knowledge of the spacecraft potential Φ_s is required for correcting accurately thermal ion measurements on Interball-2. The determination of Φ_s is based on the balance of currents between escaping photoelectrons and incoming plasma electrons. A three-dimensional model of the potential structure surrounding Interball-2, including a realistic geometry and neglecting the space-charge densities, is used to find, through particle simulations, current-voltage relations of impacting plasma electrons $I_e(\Phi_s)$ and escaping photoelectrons $I_{ph}(\Phi_s)$. The inferred relations are compared to analytic relationships in order to quantify the effects of the spacecraft geometry, the ambient magnetic field $\boldsymbol{B_0}$ and the electron temperature T_e. We found that the complex geometry has a weak effect on the inferred currents, while the presence of $\boldsymbol{B_0}$ tends to decrease their values. Providing that the photoemission saturation current density J_{ph0} is known, a relation between Φ_s and the plasma density N_e can be derived by using the current balance. Since J_{ph0} is critical to this process, simultaneous measurements of N_e from Z-mode observations in the plasmapause, and data on the potential difference $\Phi_s - \Phi_p$ between the spacecraft and an electric probe (p) are used in order to reverse the process. A value $J_{ph0} \cong 32\,\mu\mathrm{A\,m}^{-2}$ is estimated, close to laboratory tests, but less than typical measurements in space. Using this value, N_e and Φ_s can be derived systematically from electric field measurements without any additional calculation. These values are needed for correcting the distributions of low-energy ions measured by the Hyperboloid experiment on Interball-2. The effects of the potential structure on ion trajectories reaching Hyperboloid are discussed quantitatively in a companion paper.

Key words. Space plasma physics (charged particle motion and acceleration; numerical simulation studies; spacecraft sheaths, wakes, charging)

Correspondence to: M. Bouhram
(mehdi.bouhram@cetp.ipsl.fr)

1 Introduction

The charging of a conducting spacecraft in sunlight and its influence on low-energy plasma measurements are long-standing problems in magnetospheric physics, particularly when the spacecraft body potential Φ_s is comparable to the measured plasma energies. Previous studies based on electric field measurements showed that typical values of Φ_s range from a few volts positive in the inner magnetosphere up to 50 V in the tail lobes (Pedersen, 1995). Primarily, ions with energies lower than Φ_s are repelled by the spacecraft, while ions with higher energies may reach the instruments, but at shifting energies. Consequently, only a fraction of the ion population is measured. Furthermore, the potential can enhance or decrease the number of particles collected through the influence of the electric fields in the spacecraft sheath on the particle trajectories. Concerning the Interball-2 spacecraft, electric-field measurements in the polar regions show that Φ_s ranges from 0 up to 12 V (Torkar et al., 1999). The Hyperboloid experiment (Dubouloz et al., 1998), on board Interball-2, is devoted to measure three-dimensional distributions of low-energy ions ($<$ 80 eV). Since the energy of the measured ions is comparable to the typical values of Φ_s,

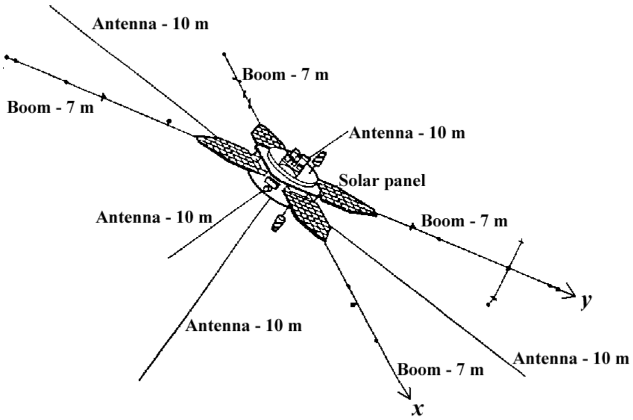

Fig. 1. Geometric structure of the Interball-2 satellite. The main body is a cylinder (radius 0.75 m, height 1.60 m) along the z-axis. Four flat solar panels looking like petals, are located in the $x-y$ plane with extended booms at the end of each panel. Four other antennas (length 10 m) are located in a plane parallel to the $x-y$ plane. A monopole (length 10 m) is inclined at 5° to the z-axis. The spacecraft spins around the z-axis, which is sunward directed. Therefore, the sunlit parts of the spacecraft are the surfaces perpendicular to the z-axis, i.e. the four solar panels and the top cylindrical surface.

a knowledge of Φ_s and the three-dimensional potential distribution around the spacecraft body are essential for correcting ion distributions recorded by Hyperboloid. These concerns are especially relevant to ion measurements when the spacecraft enters in polar regions, where ion mean energies may be very low.

The value of Φ_s is determined by the balance of currents associated with ambient electrons and ions impacting on the spacecraft body surface and photoelectrons emitted from it, which can be expressed as (Garrett, 1981):

$$I_{ph} - I_e + I_{se} + I_i = 0\,, \tag{1}$$

where I_{ph}, I_e, I_{se} and I_i denote the currents of photoelectrons flowing to the plasma, incident plasma electrons, secondary electrons due to incident electrons, and plasma ions, respectively. For positive potentials, I_i is smaller than I_e due to the ion to electron mass ratio, and can be totally neglected. I_{se} has to be taken into account when the spacecraft enters in eclipse (Grard, 1973). Due to the fact that Interball-2 was always in sunlight beyond the plasmasphere, I_{se} is negligible in our case. Hence, Eq. (1) is reduced to:

$$I_{ph} - I_e = 0\,. \tag{2}$$

The incoming plasma electron current I_e mainly depends on Φ_s and the characteristics of the electron distribution (i.e. electron density N_e and temperature T_e). The photoelectron current-voltage relation $I_{ph}(\Phi_s)$ is also determined by the photoelectron energy distribution and the photoemission saturation current density or the photoemission production rate $J_{ph0} = I_{ph}(\Phi_s = 0)/A_s$, where A_s denotes the sunlit area of the spacecraft body.

If we consider a spherical body immersed into an unmagnetized collisionless maxwellian plasma, $I_e(N_e, \Phi_s)$ can be determined analytically (Mott-Smith and Langmuir, 1926), while an expression of $I_{ph}(\Phi_s)$ can be inferred on the basis of laboratory measurements (Grard, 1973) and in-flight investigations (see Pedersen, 1995; Nakagawa et al., 2000; Scudder et al., 2000). Using this current equilibrium as described by Eq. (2), a density-potential relation $N_e(\Phi_s)$ can be inferred. In this way, measurements of Φ_s from electric field double-probe experiments on various satellites (see Pedersen, 1995; Escoubet et al., 1997; Torkar et al., 1999) have been used as a diagnostic method to derive the plasma density N_e. These previous works assumed a simple geometry for the spacecraft body and neglected the ambient magnetic field.

In our case study, the geometric structure of Interball-2 is very complex, as described in Fig. 1. Furthermore, at Interball-2 altitudes from about 8000 up to 20 000 km, the ambient magnetic field $\boldsymbol{B_0}$ ranges from 1000 to 5000 nT, corresponding to an electron gyroradius from 0.7 to 3.4 m for an energy about 1 eV. Since these values are comparable to the spacecraft body size, the ambient magnetic field should affect the current-voltage characteristics. Therefore, the method using Eq. (2) cannot be applicable to the Interball-2 case without taking into consideration the spacecraft geometry and the ambient magnetic field $\boldsymbol{B_0}$.

Recently, a Laplace solution of the three-dimensional potential structure around the Interball-2 spacecraft was carried out by Zinin et al. (1995). The model neglects the space charge effects, but includes a realistic geometry of the spacecraft body and is especially designed for computing particle trajectories through a three-dimensional potential field. In the present paper, we use this potential structure in the presence of an ambient magnetic field $\boldsymbol{B_0}$ in order to find, through particle simulations, current-voltage relationships of incoming plasma electrons $I_e(\Phi_s)$ and escaping photoelectrons $I_{ph}(\Phi_s)$. Providing that the photoemission production rate J_{ph0} is known, a relation between the ambient density N_e and Φ_s is inferred from the equilibrium of currents by considering different values of $\boldsymbol{B_0}$. Since J_{ph0} is critical to this process, in-flight measurements of N_e and Φ_s are needed to reverse the process and estimate a value of J_{ph0} on the Interball-2 sunlit surface. The main objective of this work is to infer a systematic table of spacecraft potentials and plasma densities from electric-field double probe measurements. These values are then used in correcting the ion distributions measured by the Hyperboloid instrument on board Interball-2 through particle trajectories and for estimating the unmeasured ion densities at low energy. The ion trajectory problem is discussed in a companion paper (Hamelin et al., this issue).

The outline of the paper is as follows. A brief description of the simulation technique is given in Sect. 2. Current-voltage characteristics of $I_e(\Phi_s)$ and $I_{ph}(\Phi_s)$ and comparisons with analytic theories are described in Sect. 3. The dependence of the currents on the different parameters (e.g. magnetic field, photoemission, electron temperature) is stud-

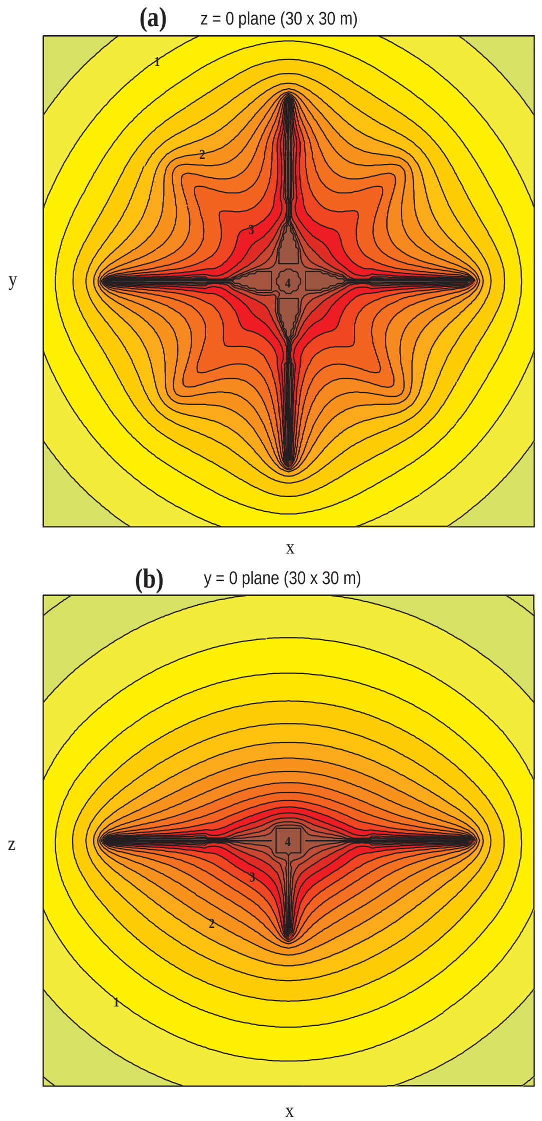

Fig. 2. Equipotential contours in V of the three-dimensional potential distribution near Interball-2 for $\Phi_s = 4$ V, and $\Phi_{\text{bias}} = -8$ V in different planes: **(a)** in the solar panels plane $x - y$, and **(b)** in a meridian plane $x - z$ through the booms.

ied. In Sect. 4, a procedure for determining the photoemission rate J_{ph0} is described. The conclusions of the paper and some discussions of the results are given in Sect. 5.

2 Model description

2.1 A three-dimensional model of the potential distribution

The Interball-2 satellite is modelled according to the drawing in Fig. 1. The Hyperboloid instrument was included in the model in order to study the electric-field perturbations on thermal ion trajectories reaching the instrument. It is also important to note that a bias potential $\Phi_{\text{bias}} = -6$ (from August 1996 to April 1997) or -8 V (from April 1997 to September 1998) was applied between the instrument and the spacecraft body in order to clamp the instrument potential to the plasma potential. The effect of potential distribution on ion trajectories reaching the Hyperboloid instrument is discussed by Hamelin et al. (this issue).

The Laplace equation solved to calculate the 3D potential distribution is linear, so that the potential distribution corresponding to any set of spacecraft and Hyperboloid potentials can be deduced from the two basic cases:

- spacecraft potential = 1 and Hyperboloid potential = 0, giving a normalized solution $u_S(\boldsymbol{r})$;
- spacecraft potential = 0 and Hyperboloid potential = 1, giving a normalized solution $u_H(\boldsymbol{r})$.

The potential solution $\Phi(\boldsymbol{r})$ from the Laplace equation can be then expressed as:

$$\Phi(\boldsymbol{r}) = \Phi_s u_s(\boldsymbol{r}) + (\Phi_s + \Phi_{\text{bias}}) u_H(\boldsymbol{r}) , \tag{3}$$

where Φ_s is the floating spacecraft potential in V.

Since the shape of the Interball-2 satellite is very extended, an accurate description of such a geometric structure requires the use of several grids. First a coarse grid (sizes: $\pm 40 \times \pm 40 \times \pm 30$ m, grid spacing: 0.5 m) is defined in the whole of the simulation domain Σ. Second a finer grid (sizes: $\pm 13 \times \pm 13 \times \pm 13$ m, grid spacing: 0.25 m) overhangs the first grid and defines a subdomain Ω on Σ. The internal bound of Ω corresponds to the spacecraft body surface. Finally a third grid (sizes: $\pm 5 \times \pm 5 \times \pm 1.5$ m, grid spacing: 0.025 m), finer than the second grid, defines a subdomain ω on Ω. The spacecraft body is centered inside each domain. The method used to solve the Laplace equation is based on an especially designed multi-grid algorithm. Details of the method are described in Zinin et al. (1995, 1998).

Figure 2 shows an example of equipotential contours of the 3D potential structure for a given value of Φ_s. The spatial extent of the potential structure from the center of the body is about 15 m in the $x - y$ plane and 10 m along the z-direction. We can see in the $x - y$ plane wings of positive potentials extended along diagonal directions. These wings are due to the electric antennas located below the solar panels at $z = -0.6$ m (see Fig. 1). The corresponding 3D electric-field model was used in calculating particle trajectories.

2.2 Current calculations

This section describes the method of calculating the electron and photoelectron current-voltage characteristics. Since the potential distribution is not calculated self-consistently, electrons and photoelectrons can be computed separately.

The ambient electrons are simulated by using a reservoir which blankets the simulation system Σ, and contains a drifting maxwellian electron population with a density N_e, and a temperature T_e. The thickness of the wall of the particle reservoirs is chosen to be sufficiently large in order to describe correctly the velocity distribution. A fixed number of electrons is kept inside the reservoir in order to conserve the electron density N_e inside Σ. Two values of T_e

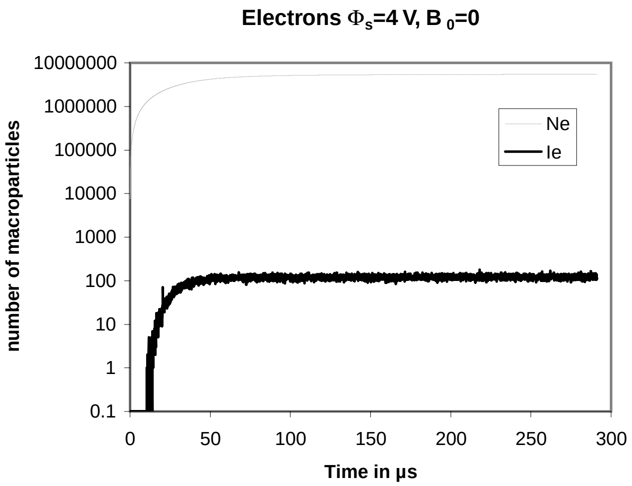

Fig. 3. Temporal evolution of collected current (thick curve, I_e) and electron density (thin curve, N_e) in macroparticle unit, for $\Phi_s = 4$ V, $T_e = 1$ eV and without magnetic field. The electron current is obtained by counting the number of macroparticles impacting the spacecraft body surface during a time step.

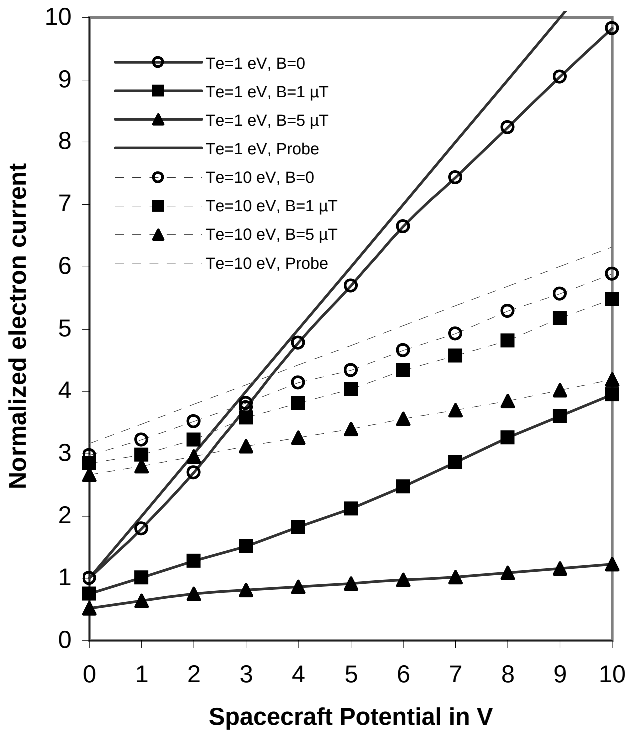

Fig. 4. Electron current-voltage characteristics for electron temperatures of $T_e = 1$ eV (solid) and $T_e = 10$ eV (dashed), for $\boldsymbol{B_0} = 0$ (circles), $\boldsymbol{B_0} = 1\,\mu$T (squares) and $\boldsymbol{B_0} = 5\,\mu$T (triangles). The two other curves correspond to the characteristic for a small Langmuir probe. All the characteristics are normalized with respect to the electron current for $T_e = 1$ eV, $\boldsymbol{B_0} = 0$ and $\Phi_s = 0$.

are considered: 1 and 10 eV, corresponding to thermal populations, while the suprathermal electron populations are not computed in our model. Therefore, this model can be applied only when the satellite travels in regions where the thermal plasma is dominant. This is the case in most of the regions, but not always, especially above aurora, where the electron thermal density can be lower than the density of energetic particles.

The photoelectrons are uniformly emitted from all the sunlit parts of the spacecraft body, and are distributed in velocity according to a maxwellian distribution with a temperature $T_{ph} = 1.5$ eV (Grard, 1973) and a saturation current density J_{ph0}. In some works based on in-flight measurements, such as Escoubet et al. (1997) or Nakagawa et al. (2000), an additional term is found in the photoelectron current for potentials greater than about 10 V. Since Φ_s is less than 12 V in our case (Torkar et al., 1999), this term is not needed in the calculations.

Each particle (electron or photoelectron) is characterized by a negative charge q_e, and a mass m_e. The particle trajectories are performed by solving the equation of motion of computer particles (electrons and photoelectrons) given by:

$$m_e \frac{d\boldsymbol{V}}{dt} = q_e\big(\boldsymbol{E}(\boldsymbol{r}) + \boldsymbol{V} \times \boldsymbol{B_0}\big)\,, \tag{4}$$

where $\boldsymbol{B_0}$ is the ambient magnetic field and $\boldsymbol{E}$ is the electric field due to the spacecraft charging. The particle motions were advanced in each time step Δt using a leapfrog integration technique. The electric field $\boldsymbol{E}(\boldsymbol{r})$ was obtained from the 3D potential solution $\Phi(\boldsymbol{r})$ from the Laplace equation. $\boldsymbol{E}(\boldsymbol{r})$ was interpolated with a scheme which provides a field accuracy of about 10^{-4} (Hamelin et al., this issue).

3 Numerical results

Particle trajectories were computed by using a Laplace solution for the 3D potential field, as described in Sect. 2. The main plasma parameters are summarized in Table 1. Several values of the floating spacecraft potential Φ_s have been considered, ranging from 0 to 10 V. The bias potential Φ_{bias} applied between Hyperboloid and the spacecraft body is -8 V. However, the Hyperboloid area is insignificant compared to the spacecraft body area for disturbing the electron and photoelectron current-voltage relations. We performed calculations with and without ambient magnetic field $\boldsymbol{B_0}$, in order to separate geometric and magnetic effects on the currents. The magnitude of $\boldsymbol{B_0}$ ranges from 1 to 5 μT, corresponding to altitudes about 20 000 and 8000 km, respectively. When the satellite travels from the dayside to the nightside auroral zone, the angle α between $\boldsymbol{B_0}$ and the solar panels ($x - y$ plane) ranges from $-30°$ to $30°$. In our simulations, $\boldsymbol{B_0}$ is contained in the $x - z$ plane and different values of α are studied, as listed in Table 1. Using analytic calculations, Escoubet et al. (1997) pointed out that in a tenuous plasma ($N_e < 1\,\text{cm}^{-3}$), the electron temperature T_e may act as a sensitive parameter in determining the relation between N_e and Φ_s. Since N_e may be lower than $1\,\text{cm}^{-3}$ when Interball-2 enters in polar regions, it is necessary to study the effect of

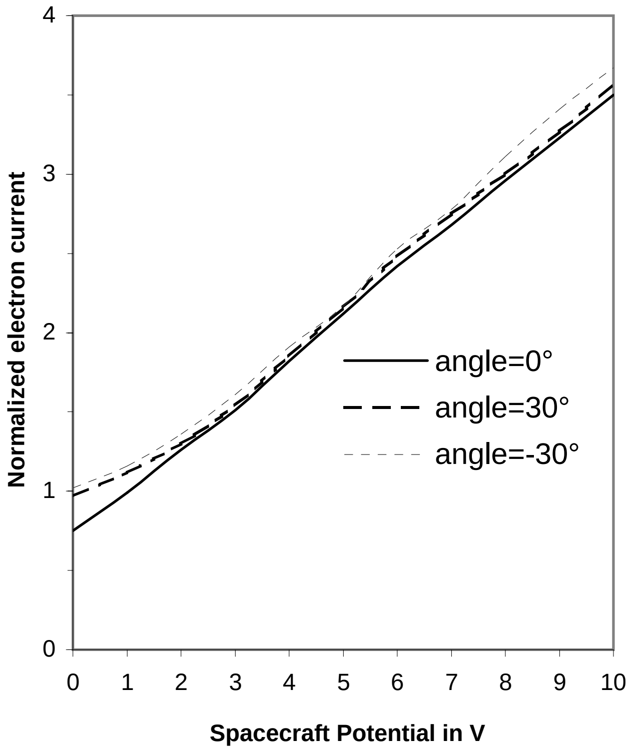

Fig. 5. Normalized electron current-voltage characteristics for $T_e = 1\,\mathrm{eV}$, $\boldsymbol{B_0} = 1\,\mu\mathrm{T}$ and different values of the angle α between $\boldsymbol{B_0}$ and the $x - y$ plane: $\alpha = -30°$ (thin dashed curve), $\alpha = 0°$ (solid curve) and $\alpha = 30°$ (thick dashed curve).

T_e on the incoming electron current I_e.

3.1 Incoming plasma electron current-voltage relation

The simulation for ambient electrons starts at $t = 0$ with an empty volume. When $t > 0$, the electrons are simulated with the reservoir blanketing the volume, and progressively filling the box. Figure 3 shows the time history of electron collection by the spacecraft and the total electron density, as seen from a particular run. It took here about $70\,\mu\mathrm{s}$ for the collected current and the ambient density to reach a quasi-steady state, which corresponds roughly to the average time for an electron from the reservoir to reach the spacecraft body across the simulation system. Electron current-voltage relationships were established by repeating simulations, for various values of $\boldsymbol{B_0}$ and T_e. Figure 4 shows the resulting curves for $\alpha = 0$.

3.1.1 Geometrical effects

The collected current without magnetic field (circles) can be compared to the current collected by an electrostatic probe with sizes smaller than the electron Debye length and given by (Garrett, 1981):

$$Is_e = I_{e0}\big(1 + \Phi_s/T_e\big)\,, \tag{5}$$

Table 1. List and values of numerical parameters used in the simulations

Definition	Notation	Value(s)
Spacecraft body potential	Φ_s	0–10 V
Ambient magnetic field	B_0	0, 1, 5 μT
Angle between $\boldsymbol{B_0}$ and the x-axis	α	-30, 0, 30°
Electron temperature	T_e	1–10 eV
Photoelectron temperature	T_{ph}	1.5 eV
Electron gyroradius	ρ_e	0.7–11 m
Photoelectron gyroradius	ρ_{ph}	0.9–4.3 m
Electron gyrofrequency	f_{ce}	27–132 kHz
Simulation time step	Δt	5.7 10^{-8} s

where I_{e0} denotes the electron thermal current given by:

$$I_{e0} = 0.026 A_T N_e \sqrt{T_e}\,. \tag{6}$$

This current corresponds for a maxwellian distribution to the electron current collected by a body at the plasma potential ($\Phi_s = 0$). A_T is the total spacecraft body area about $32\,\mathrm{m}^2$ for Interball-2, N_e is the plasma density in cm^{-3}, and T_e is the electron temperature in eV. The curve for $\boldsymbol{B_0} = 0$ is very close to the curve corresponding to Eq. (5). This points out that the electron collected current is not sensitive to complex geometrical effects.

3.1.2 Magnetic field and electron temperature effects

For $T_e = 1\,\mathrm{eV}$, the collected currents for $\boldsymbol{B_0} = 1\,\mu\mathrm{T}$ (squares) and $\boldsymbol{B_0} = 5\,\mu\mathrm{T}$ (triangles) are smaller than the collected current in an unmagnetized medium. This effect has been already identified in previous theoretical and numerical works of current collection by a probe in a magnetized plasma (see Laframboise and Sonmor, 1993; Singh et al., 1994). The electrons collected by the body come from a bunch of field lines forming a cylindrical volume aligned with the magnetic shadow of the body, the transverse size depending mainly on the electron gyroradius for moderate potentials. For $T_e = 10\,\mathrm{eV}$, the electron gyroradius becomes greater than the spacecraft dimensions, and therefore the collected currents for $\boldsymbol{B_0} = 1\,\mu\mathrm{T}$ (squares) and $\boldsymbol{B_0} = 5\,\mu\mathrm{T}$ (triangles) are found closer to the collected current in an unmagnetized medium. This means that for $T_e > 10\,\mathrm{eV}$ and altitudes above 19 000 km, electrons can be considered as unmagnetized.

Figure 5 shows the plasma electron current for $\boldsymbol{B_0} = 1\,\mu\mathrm{T}$ and different values of α. For any value of Φ_s, we found a difference on the currents of about less than 10%. This points out that for the angular range considered, there is a minor effect in the orientation of $\boldsymbol{B_0}$.

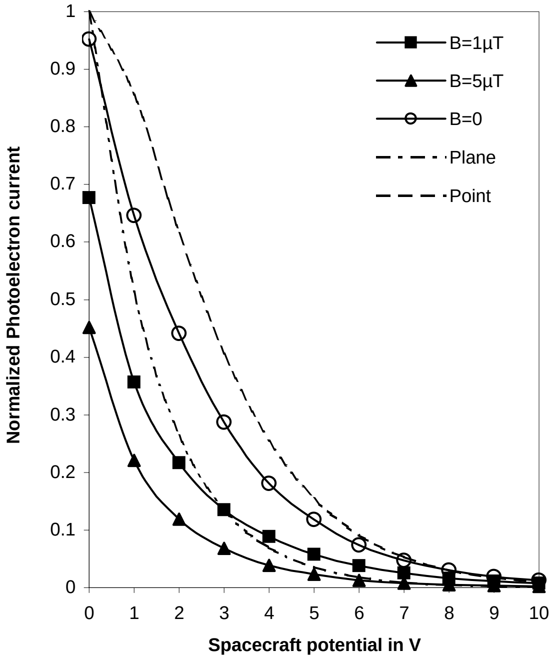

Fig. 6. Photoelectron current-voltage characteristics for $B_0 = 0$ (circles), $B_0 = 1\,\mu$T (squares) and $B_0 = 5\,\mu$T (triangles). The dashed and dash-dot curves display the currents ejected from a point source and from a planar surface, respectively. All the curves are normalized with respect to the photoelectron saturation current.

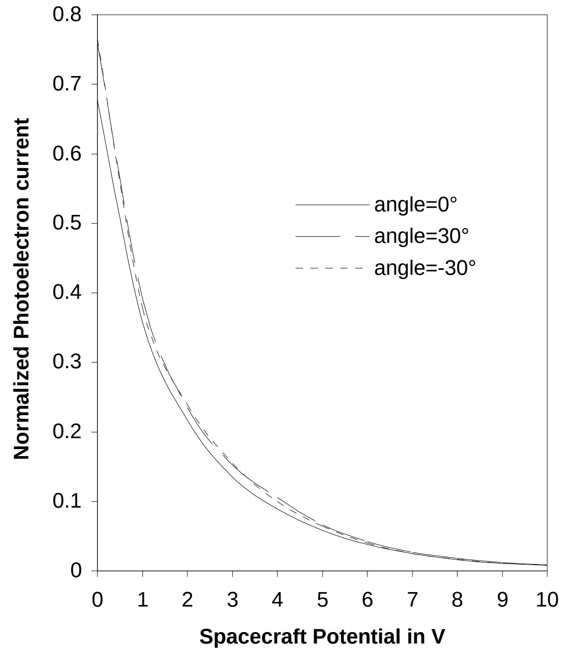

Fig. 7. Normalized photoelectron current-voltage characteristics for $B_0 = 1\,\mu$T and different values of the angle α between B_0 and the $x - y$ plane: $\alpha = -30°$ (dotted curve), $\alpha = 0°$ (solid curve) and $\alpha = 30°$ (dashed curve).

3.2 Escaping photoelectron current-voltage relation

The simulation for emitted photoelectrons starts at $t = 0$ by distributing uniformly a maxwellian population on the spacecraft sunlit surfaces. When $t > 0$, the photoelectron motion is followed by solving Eq. (4) for each computer particle. For a particular run, $I_{ph}(\Phi_s)$ is determined by the fraction of photoelectrons which reached the ambient plasma by leaving the simulation domain Σ. Figure 6 shows the resulting photoelectron current-voltage characteristics for $\alpha = 0°$, and different values of $\boldsymbol{B_0}$.

3.2.1 Geometrical effects

The ejected current for $\boldsymbol{B_0} = 0$ (circles) is compared to the currents ejected from a small spherical electrostatic sample or a point source (dashed curve) and from a planar surface (dash-dot), given by (Grard, 1973):

Small sample: I_{Sph}

$$= A_S J_{ph0}\left(1 + \Phi_s/T_{ph}\right) \exp\left(-\Phi_s/T_{ph}\right) \qquad (7)$$

Planar surface: $$I_{Pph} = A_S J_{ph0} \exp\left(-\Phi_s/T_{ph}\right), \qquad (8)$$

where J_{ph0} is the photoelectron production rate, and $A_S = 12\,\mathrm{m}^2$ is the total sunlit area. The ejected current is maximum in the point source case, when the spacecraft body size is lower than the photoelectron Debye length, as previously reported by Grard (1973). In the point source case, the equipotential surfaces are spherical, and therefore the photoelectrons are always emitted parallel to the electric field lines, and are reflected at a distance depending on their energy and not on the direction along which they have been emitted. The situation is somewhat different in the planar probe case: the equipotential surfaces are then planar, and therefore the distance at which a photoelectron is reflected also depends on the orientation of the emitted velocity vector. Therefore, all the photoelectrons of energies just higher than Φ_s can escape into the plasma in the point-source case, against only photoelectrons emitted close enough to the perpendicular direction in the planar surface case. This results for a given spacecraft body potential in the velocity phase space, in a lower number of ejected particles for a planar surface. The case of a spacecraft (e.g. Interball-2) is obviously intermediate between these two extreme cases.

3.2.2 Magnetic field effects

The ejected current-voltage characteristics for $\boldsymbol{B_0} = 1\,\mu$T (squares) and $\boldsymbol{B_0} = 5\,\mu$T (triangles) are smaller than the ejected currents in an unmagnetized medium. By taking, for example, $\Phi_s = 4$ V and $\boldsymbol{B_0} = 0$, about 18% of the photoelectrons leave the simulation box. This fraction decreases down to 9% and 4% for $\boldsymbol{B_0} = 1\,\mu$T and $\boldsymbol{B_0} = 5\,\mu$T, respectively. This is due to the gyration motion of photoelectrons curving some trajectories back to the spacecraft body, since the photoelectron gyroradius is less than the spacecraft sizes. For this reason, when $\boldsymbol{B_0}$ increases, a significant part of the photoelectron distribution returns back to the spacecraft body surface. This effect acts as an additional process

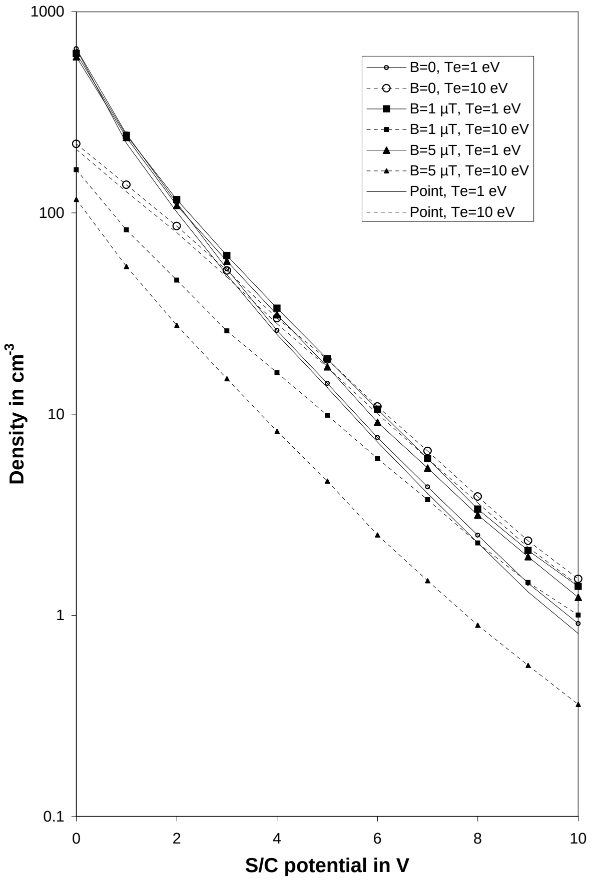

Fig. 8. Relations between the floating spacecraft potential and the plasma density $N_e(\Phi_s)$ for $B_0 = 0$ (circles), $B_0 = 1\,\mu$T (squares) and $B_0 = 5\,\mu$T (triangles). The solid and dashed fitted curves corresponding to $T_e = 1$ eV and $T_e = 10$ eV, respectively.

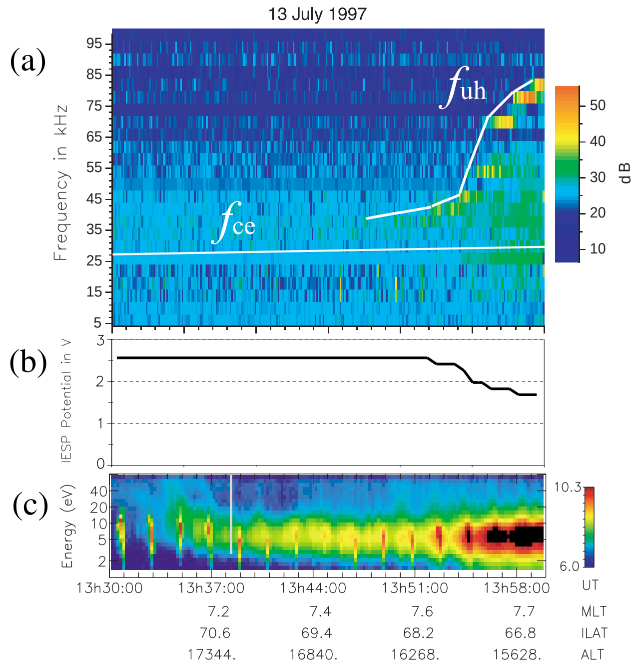

Fig. 9. Interball-2 data obtained on 13 July 1997 between 13:30 and 14:00 UT, around the plasmapause. From top to bottom: **(a)** wave spectrogram in dB from the POLRAD electric (Y) antenna, **(b)** spacecraft potential measurements in V with respect to the electric probes from the IESP experiment, **(c)** H^+ ion fluxes in $(m^2\,eV\,s\,sr)^{-1}$ versus time and energy from Hyperboloid.

on the photoelectrons with energies below Φ_s and returning to the spacecraft.

Figure 7 shows the photoelectron current for $\boldsymbol{B_0} = 1\,\mu$T and different angles between $\boldsymbol{B_0}$ and the solar panel plane $x-y$. For $\alpha = \pm 30°$, the net photoemission current $I_{ph}(\Phi_s)$ is found to be about 10% higher than in the case of $\alpha = 0°$. This points out that in our case, the orientation of $\boldsymbol{B_0}$ plays a minor role in calculating $I_{ph}(\Phi_s)$.

3.3 Density-potential relation

In space, the spacecraft potential Φ_s floats with respect to the ambient plasma conditions, as described by the balance of currents in Eq. (2). By using the current-voltage characteristics derived above, Eq. (2) provides a relationship between Φ_s and the various ambient parameters, providing that the full emitted photoelectron current density or the photoemission production rate on the spacecraft sunlit surface is known. Figure 8 shows the resulting $N_e(\Phi_s)$ relations for different values of $\boldsymbol{B_0}$. The cases where $\boldsymbol{B_0}$ is not in the solar panel plane $x-y$ are not displayed in Fig. 8, but these cases are discussed in the next section. We took a photoemission production rate J_{ph0} about 50 μA m^{-2}, which corresponds to the typical value inferred for previous magnetospheric missions (Pedersen, 1995; Escoubet et al., 1997). The unmagnetized curves are compared to the analytical solution for an unmagnetized point source with the same total area, as obtained by setting Eq. (5) equal to Eq. (7) and solving for N_e:

$$N_e(\mathrm{cm}^{-3}) = \frac{A_S J_{ph0}}{0.026 A_T \sqrt{T_e}} \frac{1+\Phi_s/T_{ph}}{1+\Phi_s/T_e} \exp\left(-\Phi_s/T_{ph}\right). \qquad (9)$$

It is found that the $N_e(\Phi_s)$ curve for $\boldsymbol{B_0} = 0$ is close to the analytical solution for a point source. This result is comprehensible, as discussed earlier in Sect. 3.2, because the effect of the complex geometrical surface is found negligible in the current calculations. For an electron temperature $T_e = 1$ eV, the effect of $\boldsymbol{B_0}$ is weak on $N_e(\Phi_s)$. This is due to the fact that both collected electron and ejected photoelectron currents are reduced under the effect of $\boldsymbol{B_0}$, but by the same factor, because T_{ph} is comparable to T_e in this case. In contrast, for $T_e = 10$ eV, ambient electrons are found as unmagnetized, while the photoelectron population remains magnetized. Therefore, for high electron temperatures, the influence of $\boldsymbol{B_0}$ is more significant in the resulting $N_e(\Phi_s)$ curves in our altitude range of interest (8000–20 000 km).

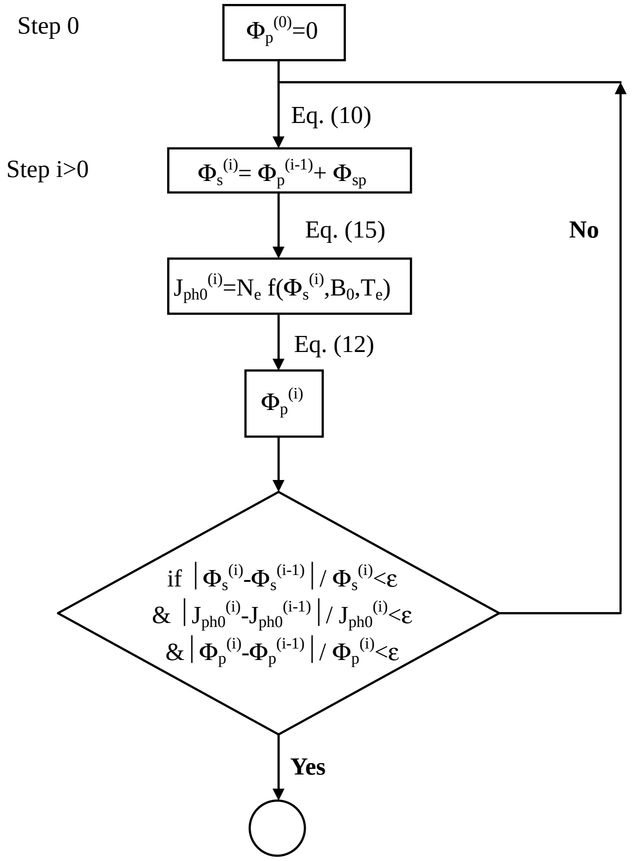

Fig. 10. Flow chart of the procedure used for determining the photoemission rate.

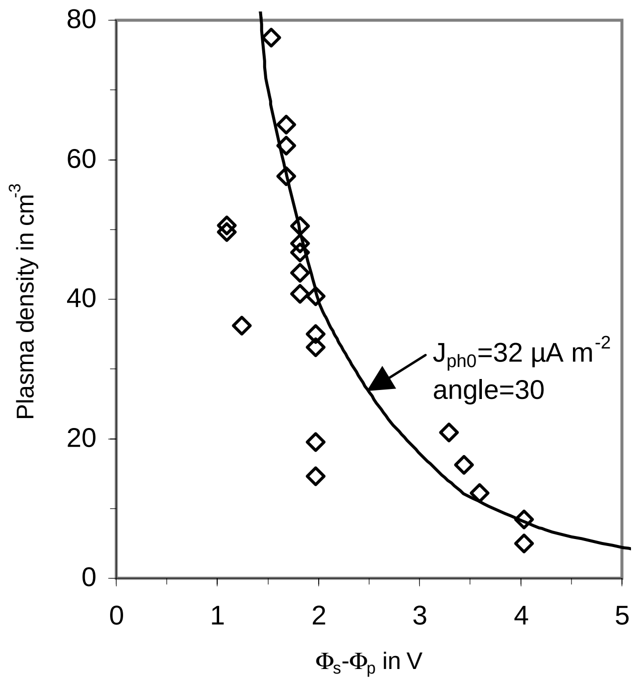

Fig. 11. Results of diagnostic measurements. The diamonds show the measurements of Φ_{sp} and N_e inferred from the IESP and POLRAD experiments, respectively. The curve corresponds to a fitted $N_e(\Phi_{sp})$ relation for $T_e = 1$ eV, $B_0 = 1\,\mu$T, $\alpha = 30°$, and by assuming a value of the photoemission rate $J_{ph0} = 32\,\mu\mathrm{A\,m}^{-2}$.

4 Applications including diagnostic measurements

4.1 Determination of the photoemission saturation current

4.1.1 Formulation of the problem

Laboratory measurements of photoemission properties of materials have been published by Grard (1973), who used the solar spectrum, together with these laboratory measurements, in order to determine photoelectron characteristics. The photoemission production rate J_{ph0} is about $30\,\mu\mathrm{A\,m}^{-2}$ for indium oxide, which is the coating material of Interball-2, and $13\,\mu\mathrm{A\,m}^{-2}$ for vitreous carbon, which is used for the electric field probes. Actually, inferred values in space are higher than from laboratory tests (Pedersen, 1995), probably because gas contamination during the pre-launch can produce a surface layer of higher photoemission rate when exposed to solar radiations over a longer period. Conversely, when the perigee altitude is lower than 1000 km, as for Interball-2, the value of J_{ph0} can be significantly reduced, presumably due to impacts of atmospheric oxygen on the spacecraft body surface (Pedersen, 1995). All these unlinked effects suggest how difficult it is to determine the variations of J_{ph0} on the spacecraft body surface along its orbit. Previous missions (Pedersen, 1995) showed that J_{ph0} ranges from $10\,\mu\mathrm{A\,m}^{-2}$ for low-altitude orbits (e.g. Viking, CRRES) to $80\,\mu\mathrm{A\,m}^{-2}$ for high-altitude orbits (e.g. ISEE, GEOS).

The aim of this section is to determine a value of J_{ph0} for the Interball-2 case. For doing so, current-voltage characteristics from the simulations showed earlier, and in-flight measurements are used.

4.1.2 Method

When the Interball-2 satellite enters the plasmapause at altitudes about 15 000 km, the electron gyrofrequency f_{ce} is about 25–50 kHz, and becomes lower than the electron plasma frequency f_{pe}. Under these conditions, cold plasma theory predicts the existence of four separately identifiable plasma wave modes at frequencies near f_{ce} and f_{pe} (Stix, 1962). These modes are the free-space right-hand extraordinary (R–X) mode, the free-space left-hand ordinary (L–O) mode, the Z-mode, and the whistler mode. The low-frequency cutoff of the R–X and L–O free-space modes are at f_{pe}, and the $R=0$ cutoff $f_R = F_{ce}/2+\left[(f_{ce}/2)^2+f_{pe}^2\right]^{1/2}$, respectively. The Z-mode is limited by the upper hybrid resonance, $f_{UH} = \left[f_{ce}^2 + f_{pe}^2\right]^{1/2}$, and the $L = 0$ cutoff, $f_L = -F_{ce}/2 + \left[(f_{ce}/2)^2 + f_{pe}^2\right]^{1/2}$. When $f_{ce} < f_{pe}$, the whistler mode propagates at frequencies below f_{ce}. In these conditions, the values of f_{pe} and f_R are very close to f_{UH}. However, only the Z-mode has a upper-frequency boundary above f_{ce}.

An example of plasmapause crossing by Interball-2 is given in Fig. 9. Panel (a) shows the electric component power spectrum, as measured by the POLRAD experiment (Hanasz et al., 1998) below 100 kHz, with a frequency resolution of 4 kHz. Figures 9b and 9c show spacecraft potential measurements by electric field double-probes, and the low-energy ion fluxes measured by the Hyperboloid experiment, respectively. The electron gyrofrequency deduced from magnetic field measurements is represented by a dashed curve in the wave spectrum. From about 13:50 UT, Interball-2 progressively enters the plasmasphere, as evidenced by a cold and dense proton population on Hyperboloid data. From about the same time, a intense emission is observed at frequencies above f_{ce}, and is tracked by crosses in the wave spectrum. Unfortunately, the magnetic wave-field components were unavailable during this time period. However, the narrow banded nature of the emission, and the fact that it is obviously of non-gyroharmonic nature, leads us to assume that this emission corresponds to the upper-hybrid resonance of the Z-mode. The plasma density can be then inferred from the formula defining f_{UH} (in kHz):

$$N_e = 0.0123\left(f_{UH}^2 - f_{ce}^2\right)\mathrm{cm}^{-3}\,. \tag{10}$$

Simultaneously, data on the spacecraft potential (panel b) are gathered by the IESP experiment (Perraut et al., 1998), which comprises double probes in order to measure the electric field as well as the potential between the spacecraft body (s) and the probe (p):

$$\Phi_{SP} = \Phi_s - \Phi_p\,. \tag{11}$$

A bias current $I_{\text{bias}} = 110\,\text{nA}$ was sent to the probes in order to clamp Φ_p to near the plasma potential. I_{bias} is added to the plasma electron current in order to compensate for the photoemission current on the probe's surface. The value of Φ_p is adjusted to maintain the current balance in the probe's surface:

$$I_{ph}\left(J_{ph0}, \Phi_p\right) - I_e\left(N_e, \Phi_p\right) - I_{\text{bias}} = 0\,. \tag{12}$$

The probe has a radius $r_s = 4\,\text{cm}$, smaller than the photoelectron Debye length (~ 1 m) and the photoelectron gyroradius (4 m). Under these conditions, the photoelectron current rejected from the probe is the same as for an unmagnetized point source:

$$I_{ph}\left(J_{ph0}, \Phi_p\right) = \pi\, r_s^2\, J_{ph0}\left(1 + \Phi_p/T_{ph}\right) \exp\left(-\Phi_p/T_{ph}\right). \tag{13}$$

For the same reasons, the electron current can be expressed as:

$$I_e\left(N_e, \Phi_p\right) = 4\pi\, r_s^2 0.026 N_e \sqrt{T_e}\left(1 + \Phi_p/T_e\right). \tag{14}$$

Using the current equilibrium on the spacecraft's surface, as inferred from numerical simulations, we obtain an additional relation between J_{ph0}, N_e and Φ_s (Sect. 3):

$$J_{ph0} = N_e f\left(\Phi_s, T_e, B_0\right). \tag{15}$$

Equations (10), (11), (12) and (15) form a system of 4 equations in 5 unknowns: N_e, T_e, Φ_s, Φ_p, and J_{ph0}. Setting one of the unknowns allows for the system to be solved. When Interball-2 travels in the plasmapause, the angle between $\boldsymbol{B_0}$ and the solar panel plane $x - y$ is about $+30°$ and the magnitude of the field is about $1\,\mu$T. Furthermore, the value of T_e in the plasmasphere is about 1 eV, as confirmed by measurements from the KM7 experiment on Interball-2 (Afonin et al., 2000). Therefore, we used for Eq. (15) the numerical relation according to these conditions, i.e. $T_e = 1\,\text{eV}$ and $\boldsymbol{B_0} = 1\,\mu\text{T}$ with an angle of $+30°$. The system of equations is solved using an iterative procedure according to the flow chart of Fig. 10. Initially, we start setting the probe potential to the plasma potential : ${\Phi_p}^{(0)} = 0$. At the first step, the spacecraft potential ${\Phi_s}^{(1)}$ is obtained from IESP measurements (Eq. 10) ${\Phi_s}^{(1)} = {\Phi_p}^{(0)} + \Phi_{sp}$. The value ${\Phi_s}^{(1)}$ is then used with the measurement of N_e to find the photoemission rate ${J_{ph0}}^{(1)}$ from Eq. (15). Then, we determine the probe potential ${\Phi_p}^{(1)}$ from Eq. (12). At the next step, the latter value of the probe potential ${\Phi_p}^{(1)}$ is added to Φ_{sp} to fix the spacecraft potential ${\Phi_s}^{(2)}$. We then iterate this process until all the unknowns (i.e ${\Phi_s}^{(i)}$, ${\Phi_p}^{(i)}$, ${J_{ph0}}^{(i)}$) converge, attaining an minimum accuracy ε.

We assumed here that the photoemission rate is nearly the same for the spacecraft body and the probe. This hypothesis was justified for previous magnetospheric missions (Pedersen, 1995), showing that the potential difference between the spacecraft body and a floating probe (i.e. no bias current applied) was found about a fraction of a volt in a wide range of plasma conditions. The calculation method also imposes the condition that J_{ph0} has to keep roughly the same value during the period of the measurements, which is clearly the case in the absence of the eclipse and due to the narrow altitude range considered.

4.1.3 Results

Figure 11 shows the values for Φ_{sp} and N_e related to conjugate measurements by IESP and Z-mode observations during the period between July 1997 and October 1997. After solving the system of equations for all the measurements, we found an average value of $J_{ph0} = 32 \pm 5\,\mu\text{A}\,\text{m}^{-2}$. We have represented in the graph the $N_e(\Phi_{sp})$ relation for $T_e = 1\,\text{eV}$ and $J_{ph0} = 32\,\mu\text{A}\,\text{m}^{-2}$. It is interesting to compare our estimated value of J_{ph0} with the values inferred from laboratory measurements and previous studies for other satellites. This value is in the range [10, $80\,\mu\text{A}\,\text{m}^{-2}$] inferred from electric field double-probe measurements on board previous missions (Pedersen, 1995; Escoubet et al., 1997; Nakagawa et al., 2000). The value $J_{ph0} = 32\,\mu\text{A}\,\text{m}^{-2}$ is very close to the value inferred from laboratory measurements (Grard, 1973) which is about $30\,\mu\text{A}\,\text{m}^{-2}$ for indium oxide surfaces. If we compare J_{ph0} to the values inferred from satellites coated in indium oxide, such as Geotail (Nakagawa et al., 2000), our value differs approximately by a factor of 2.5 ($32\,\mu\text{A}\,\text{m}^{-2}$ against $80\,\mu\text{A}\,\text{m}^{-2}$). Pedersen (1995) points out that J_{ph0} values are generally higher in space. However, the same au-

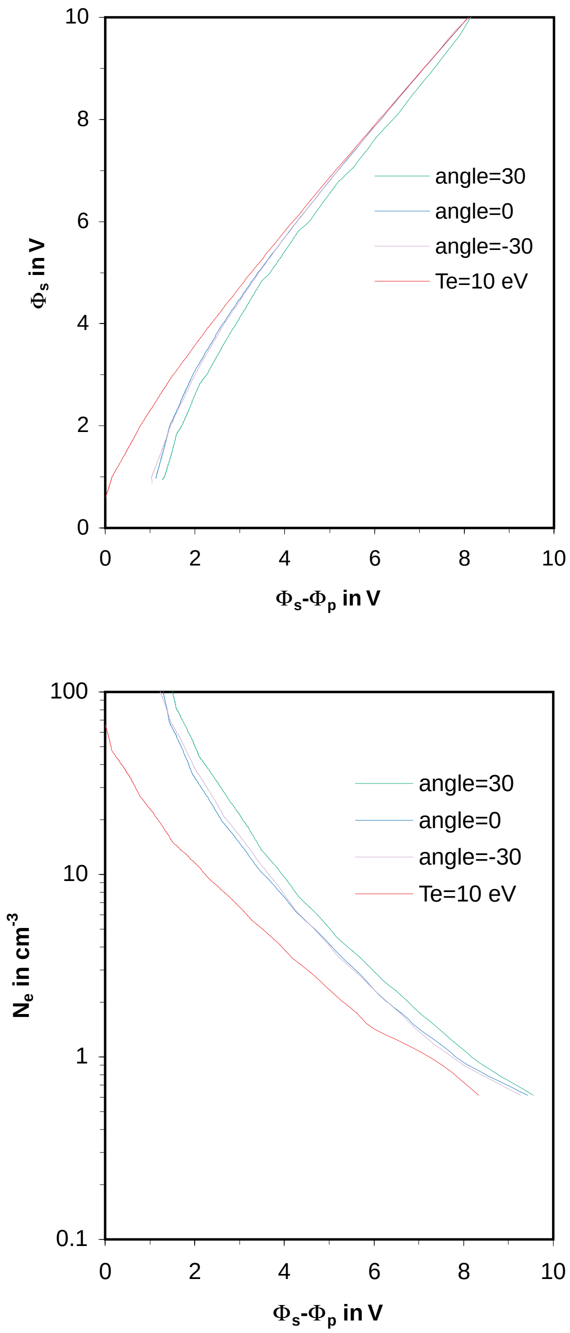

Fig. 12. Relations for $B_0 = 1\,\mu$T between: **(top)** the spacecraft-probe potential measured by IESP and the spacecraft potential with respect to the plasma, **(bottom)** the spacecraft-probe potential measured by IESP and the plasma density. The plotted curves are associated with the following parameters : $T_e = 10$ eV, $\alpha = 0°$ (red), $T_e = 1$ eV, $\alpha = -30°$ (purple), $T_e = 1$ eV, $\alpha = 0°$ (blue), and $T_e = 1$ eV, $\alpha = +30°$ (green).

thor shows that these values can be reduced for satellites having a low-altitude perigee (< 1000 km). Another possible effect on Interball-2 is that frequent gas releases (once in 12 h) used to damp the nutation of the satellite can keep J_{ph0} low (Galperin, private communication).

4.2 Spacecraft potential and density tables

A value of the photoemission production rate J_{ph0} has been deduced from in-flight measurements and simulation results, as described in the last section. Using this value, the plasma density N_e can be deduced from Φ_s by using the relations inferred numerically from Laplace simulations. Along the Interball-2 orbit, the IESP experiment provides the potential difference Φ_{sp} between the spacecraft body (s) and the electric probes (p). Therefore, it is possible to determine systematically the values of the plasma density N_e and the floating spacecraft body potential Φ_s, with respect to the plasma. In this way, Eqs. (11), (12) and (15) can be computed numerically for $J_{ph0} = 32\,\mu\mathrm{A\,m}^{-2}$, and values of Φ_{sp}, ranging from 0 to 10 V, with the following unknowns N_e, Φ_s, Φ_p and T_e. Two values of T_e are considered: $T_e = 1$ eV and $T_e = 10$ eV, and the ambient magnetic field $\boldsymbol{B_0}$ is taken to be about 1 μT, with α ranging from $-30°$ to $30°$. This magnitude of $\boldsymbol{B_0}$ corresponds to altitudes ranging from 15 000 to 20 000 km along the Interball-2 orbit.

Figure 12 shows the resulting curves of Φ_s and N_e versus Φ_{sp}. For $T_e = 1$ eV, the $\Phi_s(\Phi_{sp})$ and $N_e(\Phi_{sp})$ depend weakly on the angle α between $\boldsymbol{B_0}$ and the solar panel plane $x - y$. The floating spacecraft body potential versus Φ_{sp} is not sensitive to the electron temperature for measurements above 2 V. An asymptotic linear shape is found above 2 V. This is due to the fact that when N_e decreases very low, the electron current collected by the probe (see Eq. 14) becomes negligible in Eq. (12). Therefore, the value Φ_p insures the equilibrium between the bias current and the photoelectron current, giving a constant value of about 2 V, and Φ_s can be asymptotically expressed as:

$$\Phi_s = \Phi_{sp} + 2.0\,\mathrm{V}\,. \tag{16}$$

However, the plasma density remains more sensitive to the electron temperature T_e when Φ_{sp} is less than 4 V. This result was previously reported in Sect. 3.3, and is due to the fact that the electron population becomes unmagnetized when T_e is high (above 10 eV), modifying significantly the current equilibrium. While T_e is undetermined, N_e can be estimated only with a limited accuracy. Therefore, the electron temperature has to be taken into account when the satellite enters into regions where suprathermal electrons are observed, such as the auroral zones.

During the working periods of the IESP experiment, these diagnostic curves will be put as input parameters for determining the floating spacecraft potential with respect to the plasma. An example is given in Hamelin et al. (this issue), where the knowledge of Φ_{sp} and therefore Φ_s is used to perform both energy and angular corrections on ion distributions measured by the Hyperboloid instrument.

5 Summary

A method for determining the floating potential Φ_s of the Interball-2 spacecraft as a function of the different plasma parameters has been developed on the basis of the current balance between photoelectrons rejected from the spacecraft's sunlit surface and incoming plasma electrons. In contrast to previous works based on this method (see Pedersen, 1995; Escoubet et al., 1997), the spacecraft model is not approximated to a simple geometry and consequently, analytic formulas are not useful. In this way, current-voltage relations of escaping photoelectrons $I_{ph}(\Phi_s)$ and incoming plasma electrons $I_e(\Phi_s)$ are inferred numerically from particle trajectories in a realistic three-dimensional model of the potential distribution surrounding Interball-2 in the infinite Debye length limit (i.e. Laplace solution). By comparing the simulation results with analytic relationships, we point out that the inferred current-voltage relations are weakly modified by the complex geometrical effects. Furthermore, we have studied the dependence of the currents on the different parameters, such as the electron temperature T_e, the magnitude and the direction of the ambient geomagnetic field $\boldsymbol{B_0}$. For the orbital conditions considered, the magnitude of $\boldsymbol{B_0}$ has a more larger effect on the current-voltage relations than its orientation in the spacecraft frame. Actually, the main effect, when $\boldsymbol{B_0}$ is included, is to reduce both $I_{ph}(\Phi_s)$ and $I_e(\Phi_s)$, because of particle gyroradii comparable to the spacecraft dimensions. When $\boldsymbol{B_0}$ is fixed, the current equilibrium between $I_{ph}(\Phi_s)$ and $I_e(\Phi_s)$ provides a relation between Φ_s and the plasma parameters (electron density N_e and temperature T_e). Meanwhile, in order to obtain realistic values of I_{ph}, we need to know the photoemission rate or the saturation current density $J_{ph0} = I_{ph}(\Phi_s = 0)/A_s$, where A_s denotes the spacecraft's sunlit area. In this way, we have developed a reversed method, using in-flight measurements of N_e and the potential difference $\Phi_{sp} = \Phi_s - \Phi_p$ between the spacecraft and an electric probe. The method consists of solving, by setting $T_e = 1\,\text{eV}$, a system of four equations with N_e, Φ_s, Φ_p and J_{ph0} as unknowns. The inferred photoemission rate J_{ph0} is about $32\,\mu\text{A m}^{-2}$, comparable to laboratory predictions (Grard, 1973).

Once J_{ph0} is determined on Interball-2 and providing that $\boldsymbol{B_0}$ and T_e are known, values of the plasma density N_e and the spacecraft potential Φ_s can be found systematically from in-flight measurements of Φ_{sp}, without any analytic calculation. Measurements of $\boldsymbol{B_0}$ are currently available from DC magnetometers. The situation is somewhat different for T_e. Since measurements of T_e are not systematic, we have considered two extreme values $T_e = 1$ to $10\,\text{eV}$ in order to have an idea of the uncertainty when determining N_e and Φ_s. Such values of T_e correspond to plasma conditions where cold electron populations are dominant, such as in the polar regions or in the plasmapause. It is found that Φ_s can be inferred precisely from Φ_{sp}, while the accuracy in determining N_e is still limited.

All these results are fundamental for correcting thermal ion measurements on Interball-2. In particular on Interball-2, the knowledge of Φ_s is essential for studying the spacecraft charging effects on the ion distributions recorded by Hyperboloid, such as the distortion effects on the ion trajectories reaching the vicinity of the instrument (see Hamelin et al., this issue). Systematic estimations of Φ_s and N_e, along with angular corrections providing that measurements of Φ_{sp} are available, will be used in correcting ion distributions. Furthermore, the knowledge of N_e provides an estimation of the density of low-energy ions repelled by the potential structure and missed by the instrument. Ultimately, a Hyperboloid database will take into account these corrections for the two-year working period of the instrument.

Acknowledgements. The Interball Project was accomplished in the frame of contract N025-7532/94 with the Russian Space Agency (RKA). The Hyperboloid experiment was financially supported by CNES under the auspices of grants covering the period 1985 to 2001. The work of Y. Galperin and M. V. Veselov is supported by the RFFI grant PICS 00-02-22001. The POLRAD experiment is currently supported by the committee of the scientific research in Poland, grant no. 2 P03C 003 16.

The Editor in Chief thanks P. Escoubet and another referee for their help in evaluating this paper.

References

Afonin, V. V., Akentieva, O. S., and Smilauer, J.: Interball-2 measurements of the components of thermal and suprathermal plasma ($E < 15\,\text{eV}$) in high-latitude regions of the magnetosphere at altitudes of 2–3 earth radii, Cosmic Res., 38, 515, 2000.

Dubouloz, N., Berthelier, J.-J., Malingre, M., Girard, L., Galperin, Y., Covinhes, J., Chugunin, D., Godefroy, M., Gogly, G., Guérin, C., Illiano, J.-M., Kossa, P., Leblanc, F., Legoff, F., Mularchik, T., Paris, J., Stzepourginski, W., Vivat, F., and Zinin, L.: Thermal ion measurements on board Interball Auroral Probe by the Hyperboloid experiment, Ann. Geophysicae, 16, 1070–1086, 1998.

Escoubet, C. P., Pedersen, A., Schmidt, R., and Lindqvist, P. A.: Density in the magnetosphere inferred from ISEE 1 spacecraft potential, J. Geophys. Res., 102, 17 595, 1997.

Garrett, H. B.: The charging of spacecraft surfaces, Rev. Geophys. Space Phys., 19, 577–516, 1981.

Grard, R.: Properties of the satellite photoelectron sheath derived from photoemission laboratory measurements, J. Geophys. Res., 78, 2873, 1973.

Hamelin, M., Bouhram, M., Dubouloz, N., Malingre, M., Grigoriev, S. A., and Zinin, L. V.: Electrostatic interaction between Interball-2 and the ambient plasma. 2 Influence on the low energy ion measurements with Hyperboloid, Ann. Geophysicae, this issue, 2001.

Hanasz, J., Schreiber, R., de Feraudy, H., Mogilevsky, M., and Romantsova, T. V.: Observations of the upper frequency cutoffs of the auroral kilometric radiations, Ann. Geophysicae, 16, 1097–1104, 1998.

Laframboise, J. G. and Sonmor, L. J.: Current collection by probes and electrodes in space magnetoplasmas: A review, J. Geophys. Res., 98, 337, 1993.

Mott-Smith, H. and Langmuir, I.: The theory of collectors in gaseous discharges, Phys. Rev., 28, 727, 1926.

Nakagawa, T., Ishii, T., Tsuruda, K., Hayakawa, H., and Mukai, T.: Net current density of photoelectrons emitted from the surface of the GEOTAIL spacecraft, Earth Planets Space, 52, 283, 2000.

Pedersen, A.: Solar Wind and magnetosphere plasma diagnostics by spacecraft electrostatic potential measurements, Ann. Geophysicae, 13, 118–129, 1995.

Perraut, S., Roux, A., Darrouzet, F., de Villedary, C., Mogilevsky, M., and Lefeuvre, F.: ULF wave measurements onboard the Interball auroral probe, Ann. Geophysicae, 16, 1105–1116, 1998.

Scudder, J. D., Cao, X., and Mozer, F. S.: Photoemission current-spacecraft voltage relation: Key to routine, quantitative low-energy plasma measurements, J. Geophys. Res., 105, 21 281, 2000.

Singh, N., Vashi, B. I., and Leung, W. C.: Three-dimensional numerical simulation of current collection by a probe in a magnetized plasma, Geophys. Res. Lett., 9, 833, 1994.

Stix, T. H.: The theory of plasma waves, McGraw-Hill, New York, 1962.

Torkar, K., Jeszenski, H., Veselov, M. V., Perraut, S., Dubouloz, N., Escoubet, C. P., and Galperin, Y. I.: Spacecraft potential measurements on board Interball-2 and derived plasma densities, Cosmic. Res., 37, 606, 1999.

Zinin, L. V., Galperin, Y. I., Gladyshev, V. A., Grigoriev, S. A., Girard, L., and Mularchik, T. M.: Modelling of the anisotropic thermal plasma measurements of the energy-mass-angle ion spectrometers onboard a charged satellite, Cosmic Res., 33, 511, 1995.

Zinin, L. V., Galperin, Y. I., Grigoriev, S. A., and Mularchik, T. M.: On measurements of polarization jet effects in the outer plasmasphere, Cosmic Res., 36, 42–52, 1998.